Far Field Estimations and Simulation Model Creation from Cable Bundle Scans

D. Rinas, S. Niedzwiedz, S. Frei
Dortmund University of Technology
Dortmund, Germany
denis.rinas@tu-dortmund.de
stephan.frei@tu-dortmund.de

Abstract— **The emission level of automotive systems is often governed by the cable harness, it is often the dominant radiating structure and determines the position of resonances. The established field measurement methods according CISPR 25 for evaluation of emissions suffer from the need to use large anechoic chambers. Furthermore measurement data can not be used for simulation model creation in order to compute the overall fields radiated from a car. In this paper a simple method to determine the far-fields and a simulation model of a radiating cable bundle from near-field measurements is proposed. The method measures the electromagnetic fields at several points near to a cable bundle. Measurements are done in time domain in order to get phase information, to reduce measurement time, and to correlate different measurement data sets. From the field measurement data an equivalent current distribution in a cable bundle can be computed. With this information a simulation model of the setup can be generated, far-field estimations can be done.**

I. INTRODUCTION

Electromagnetic Compatibility plays an important role in the development of automotive electronic systems. The integrated Electronic Control Units (ECUs) and especially the mainly used unshielded cable bundles are sources for electromagnetic emissions.

Standardized component field measurement methods, like the ALSE antenna method provided in CISPR 25 [1] for evaluation of electro-magnetic emissions from automotive systems, suffer from the need of large and expensive anechoic chambers. Also a single field strengths value is often not sufficient to characterize the EMI behavior of a complex system. Furthermore it is not possible to use the measurement data for behavioral model creation for simulation. Having simulation models, a statement about the radiating electromagnetic fields can already be made in early phases of development.

Basically the electromagnetic emission must be distinguished in the emission from circuit boards and their housing and the emission from the connecting cable bundles.

To be able to determine the radiated far fields it is necessary to transfer the radiating ECU structure and the attached cables into an equivalent behavioral model with reduced complexity. Knowing the fields in an indefinitely extended e plane above the test object all information is available to calculate any field vector above this plane [2]. From theoretical point of view this would be sufficient to calculate the far fields. There are several problems with such an approach. E.g. accuracy of measurements is limited and accuracy of field calculation can be low. It is better to try to solve the inverse problem and thus to identify by the measured field important properties of the test object. This approach is discussed in [3], [4], [5] and [12]. Focus is placed mainly on PCBs.

However, considering the small structure size of most automotive PCB and housings and compare it with the wavelengths in the frequency range below 200 MHz, radiation from cables is often the dominant emission factor. To characterize complex cable bundles with standard voltage and current measurements on each single cable is often not feasible.

This paper presents a special method for estimating the emissions from cable bundles. The electromagnetic near-field at several points near a cable bundle is measured. With measured date an equivalent current distribution in the bundle is calculated and a simulation model can be created. The generated model enables different types of post-processing e.g. far field estimations. The method can be combined with scans of the PCB and the enclosure structure, in order to determine the full system behavior and to create behavioral models for large system simulations.

Accurate source identification requires phase information [12], most groups working on scanning methods don't discuss this problem. In [3] an approach based on frequency domain measurements is presented. Disadvantages of the method are the high complexity and measurement time.

In this paper a time domain approach with a standard oscilloscope is presented. Advantages are, the direct availability of the phase information, the possibility to measure 4 field components simultaneously, i.e. synchronized, and the faster simulation time.

II. SCANNING METHOD FOR SYSTEM CHARACTERIZATION

Typical automotive systems consist of one or more ECUs and their connecting cable bundles (Figure 1). Idea of the presented approach is to estimate the electro-magnetic fields of an automotive cable bundle by creating a behavioral model based on scanner-measurement data. The ECUs are considered here as black boxes, using a linear behavioral model approach. As the voltage amplitudes of RF-disturbances are often not big,

small signal approaches are valid and linear models can approximate the emission behavior of the electronic system. In the approach presented here, ECUs are considered as non radiating lumped circuits. An extension with radiating structures is possible, but not discussed in this paper.

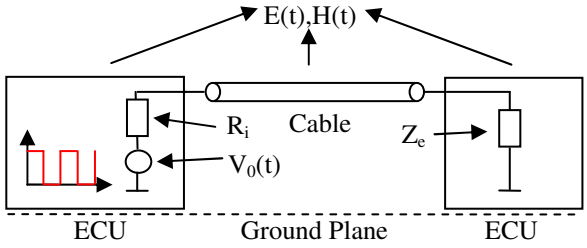

Figure 1. System to investigate

For creating the behavioral model the current distribution on cable bundle must be approximated. Complex near field data is collected at several points on lines parallel to the bundle. Therefore the measurements are done in Time Domain, followed by a transformation in Frequency Domain for further processing. With

$$I(z) = \frac{H(z)}{\frac{1}{2\pi d} - \frac{1}{2\pi(2h+d)}} \quad (1)$$

the correlation between the magnetic field and current distribution is given for a long homogeneous cable placed close above a ground plane. Where d is the distance from bundle to measured field point and h is the height of the cable bundle above the ground plane. The closer to the cable the fields are measured the higher is the accuracy of (1). The height h is also assumed to be small. The model creation process is presented in Figure 2.

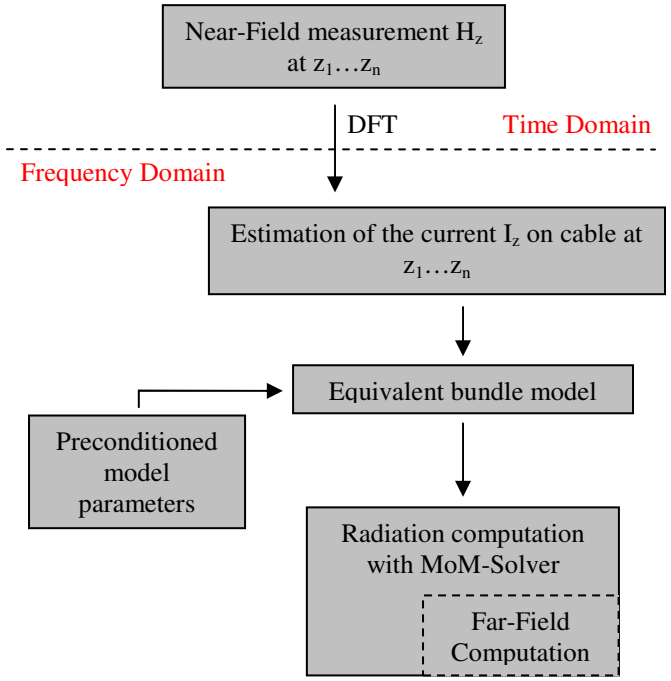

Figure 2. Process of model creation

A. *Measurement Setup*

For measuring the magnetic field a small loop antenna is used. The voltage V_i is induced by the magnetic flux through the area A of the loop.

$$V_i = -\frac{\partial}{\partial t}\int_A \vec{B}d\vec{A} \quad (2)$$

If the field is homogeneous and the probe diameter is considerably smaller than the wavelength, the flux in the loop can be considered as constant. For the magnetic field component oriented normal to the loop plane the equivalent circuit presented in Figure 3 can be drawn.

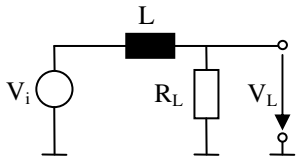

Figure 3. Equivalent circuit of magnetic field probe

The probe voltage V_L is calculated by

$$V_L = V_i \frac{Z_L}{R_L + Z_L} \quad (3)$$

Based on the measured magnetic field at position z near the cable the corresponding current on the line can be computed. For that purpose the transfer function between the measured probe voltage and the equivalent current on the line can be derived from (1, 3). The constant μ describes the relative permeability and r_s gives the loop radius of the magnetic field probe.

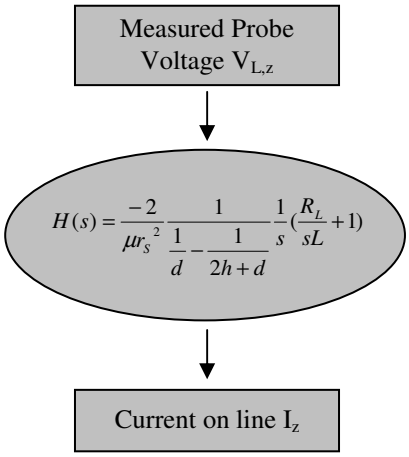

Figure 4. Transfer function for magnetic field probe

The measurement setup consists of a signal generator for feeding the cable bundle, the magnetic field probe (Figure 5) and a tripod for probe positioning. The cable under test is placed above the ground plane. The probe voltage is measured in Time Domain with a 4 channel standard oscilloscope. By synchronizing the channels and different measurement sets with a reference probe signal accurate phase information can be

obtained. Another important advantage of the Time Domain measurements is the decrease of measurement duration.

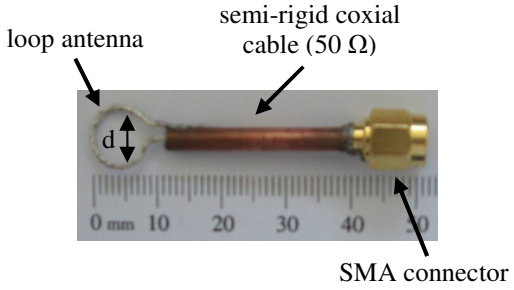

Figure 5. Magnetic field probe (diameter d ≈ 9 mm)

B. Time Domain - Frequency Domain Transformation

Time domain measurements have several advantages discussed above. For the following post-processing I_z is transformed in the frequency domain.

For obtaining the Frequency Domain information of a measured Time Domain signal the Fourier-Transformation is used. This transformation provides the complex information in a continuous Frequency Domain, from which spectrum and phase information can easily be derived. Furthermore the Fourier-Transformation is fully reversible.

$$F\{x(t)\} = X(\omega) = \int_{-\infty}^{\infty} x(t) \cdot e^{-j\omega t} dt \tag{4}$$

As the continuous Fourier-Transformation requires continuous Time Domain data it is not usable in case of digital signal processing. Therefore the Time Domain data is discretized at fixed time steps according to a chosen sampling frequency that should be identical to the scope sampling frequency.

$$\Delta t = \frac{1}{f_S} \tag{5}$$

Additionally, the chosen sampling frequency specifies the maximum frequency detectable by the Fourier-Transformation, which is limited by the Nyquist-Theorem.

$$f_{\max} \le \frac{1}{2} f_S \tag{6}$$

Hence all frequency components higher than f_{max} should be suppressed by a low-pass filter to avoid problems originating from Alias-Effect. In this case the transformation is known as Discrete Fourier Transformation (DFT)

$$F\{s(n)\} = S(k \cdot \Delta f) = \sum_{0}^{N-1} s(n \cdot \Delta t) \cdot e^{-j2\pi \frac{kn}{N}} \tag{7}$$

The DFT is working on a fixed length data sequence *s(n)* that is assumed to be repeating periodically. The length *N* of the sampling sequence hereby defines the discrete frequency resolution of the DFT.

$$\Delta f = \frac{f_S}{N} = \frac{1}{N \cdot \Delta t} \tag{8}$$

For achieving good results the frequency resolution should be chosen as an integer divider of the most interesting frequency, but in general the frequency components of a signal are not known prior to the measurement.

An efficient realization of the DFT is achieved by the Fast Fourier Transformation (FFT), which takes advantage of symmetries along roots of unity used in the calculation. Different algorithms for the FFT exist, which mainly differ in their efficiency concerning different input sequence lengths *N*.

Another aspect in the usage of the DFT is the windowing of the original sequence in Time Domain. The input sequence *s(n)* itself can be understood as part of the original measurement data windowed by a rectangular function of length *N*.

$$s(n) = x(n) \cdot w_N(n) \tag{9}$$

The multiplication of the data sequence with a window function in Time Domain corresponds to a convolution of the transformed data sequence with the transformed window function in Frequency Domain.

$$S(k) = F\{x(n)\} * F\{w(n)\} \tag{10}$$

This causes a certain distortion in the Frequency-Domain result depending on the used window function which is also known as Leakage-Effect.

To obtain the necessary precision of the frequency data used in this work, without wasting computing time, measuring time and memory, the frequency resolution Δf is carefully chosen between 0.01 and 0.1 times of the desired minimum frequency. To further optimize these efficiencies criteria the sampling frequency f_S is chosen in relation to the desired maximum frequency.

In Figure 6 measurement results of a pulsed input signal into a single cable made with a test receiver can be seen. Here the pulse has an amplitude $V_0 = 1$ V, a fundamental frequency of $f_0 = 10$ MHz, a pulse/pause ratio $t_h/t_l = 0.1$ and a rising and falling edge of $t_{r,f} = 2.5$ ns. In comparison the results from the FFT based on a Time Domain measurement are shown in Figure 7. Hence, the FFT results are very accurate. The main differences between both methods are the noise floor levels caused by the measuring device and the spectrum shape around the peaks caused by resolution bandwidth (RBW) and window shape.

As explained above the dynamics of the FFT-method mainly depend on the used sampling frequency and the duration of the measurement. Theoretically any frequency resolution below the Nyquist-frequency (6) can be achieved. The signal's shape and frequency do not have considerable effects on the result in general. A physically limiting factor to the results is set by the used measurement devices, more precise its noise floor levels and attenuations.

The difference in the amplitude values, which is quite constant along the spectrum, is explained with the measurement method itself. The test receiver measures the effective value, whereas the used FFT calculates the peak values of the Fourier components of a given signal.

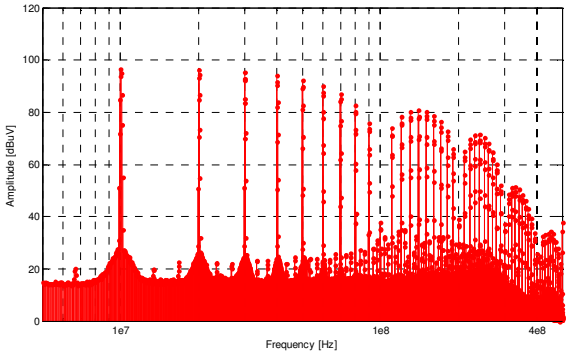

Figure 6. Signal measured with a test receiver

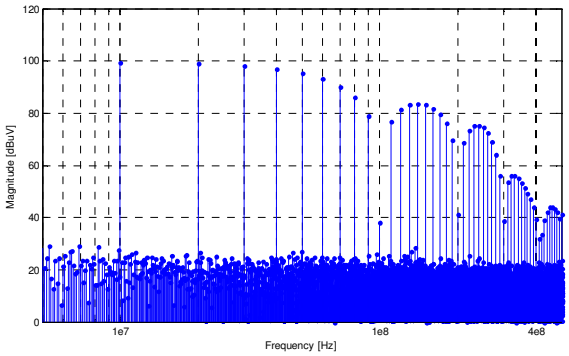

Figure 7. Signal measured in Time Domain and transformed into spectrum

C. *Equivalent Transmission Line Model*

To approximate the cable bundle behavior a single transmission line model with equivalent current distribution is generated. The presented approach is based on the lossless transmission line equations. The voltage and current at position z on the transmission line can be calculated as

$$V_z = \frac{1}{2}(V_e + ZI_e)e^{j\beta(l-z)} + \frac{1}{2}(V_e - ZI_e)e^{-j\beta(l-z)} \quad (11)$$

$$I_z = \frac{1}{2Z}(V_e + ZI_e)e^{j\beta(l-z)} + \frac{1}{2Z}(V_e - ZI_e)e^{-j\beta(l-z)} \quad (12)$$

with wave impedance Z and the propagation constant β. As shown in Figure 4 the current I_z on transmission line can be calculated from the magnetic field measurements. For model generation process some model parameters have to be predefined. These are the length l of the transmission line, the radius r of the electric conductor and the height h over ground plane [8]. Length and height are chosen corresponding to the cable bundle under test. Based on these input parameters the terminating impedance Z_e (Figure 1) can be calculated as

$$Z_e = \frac{V_e}{I_e} \quad (13)$$

where V_e and I_e are voltage and current at the end of the transmission line. For estimating V_e and I_e only two sets of data are necessary.

$$\begin{pmatrix} V_e \\ I_e \end{pmatrix} = \begin{bmatrix} a_1 & b_1 \\ a_2 & b_2 \end{bmatrix}^{-1} \cdot \begin{pmatrix} I_1(z_1) \\ I_2(z_2) \end{pmatrix} \quad (14)$$

$$a_1 = \frac{1}{2Z}(e^{j\beta(l-z_1)} - e^{-j\beta(l-z_1)}),\ b_1 = \frac{1}{2}(e^{j\beta(l-z_1)} + e^{-j\beta(l-z_1)})$$
$$a_2 = \frac{1}{2Z}(e^{j\beta(l-z_2)} - e^{-j\beta(l-z_2)}),\ b_2 = \frac{1}{2}(e^{j\beta(l-z_2)} + e^{-j\beta(l-z_2)}) \quad (15)$$

To minimize errors in the model generation process the possibility to measure a local minimum of current distribution on line must be regarded. This fact can cause a low signal-noise-ratio. Two approaches are possible here.

- The amount of data sets is increased by measuring the cable bundle at $N >> 2$ field points. N is depending on the desired maximum frequency to be measured. This leads to an over-determined system of equations. It can be solved with the method of least squares or else approximated to a sinusoidal function.
- A pre-processing scanning is done before measuring the two magnetic field points. Based on this scanning the local maxima on line are estimated and the measurements are done here.

With the predefined internal resistance of the source R_i source voltage V_0 can be computed (Figure 1).

$$V_0 = V_a \frac{Z_a + R_i}{Z_a} \quad (16)$$

$$Z_a = Z \frac{Z_e + jZ\tan(\beta l)}{Z + jZ_e\tan(\beta l)} \quad (17)$$

D. *Equivalent Dipole Model*

As described in chapter C the current distribution on a cable bundle can be estimated. Therefore measurements are done in $N >> 2$ field points on a line above the bundle and approximated to a sinusoidal function. Afterwards the resulting current distribution function is approximated by electric dipoles with dipole moment

$$M_k = I_k d_k \quad (18)$$

where I_k is the current on line element and d_k is the discretization size. The dipoles are arranged above a ground plane in height h, adopted from the cable bundle under test.

III. RESULTS

The developed methods were tested to confirm applicability. For the investigations a pulsed signal is generated. The pulse has an amplitude $V_0 = 5$ V, a fundamental frequency of $f_0 = 4$ MHz, a pulse/pause ratio $t_h/t_l = 1$ and a rising and falling edge of $t_{r,f} = 2.5$ ns. It is impressed by a 50-Ohm system.

A. *Single Conductor – Equivalent Transmission Line Model*

The cable (Figure 8) consists of a single conductor placed in the height $h = 50$ mm over a ground plane. It has a length of $l = 490$ mm and a thickness of $d = 1$ mm. It is terminated with a

Z_e = 50 Ω impedance. The predefined model parameters are adopted from the cable under test. The internal resistance of the source is set to R_i = 50 Ω. The magnetic field is measured at two positions at a height h_S = 10 mm above the cable.

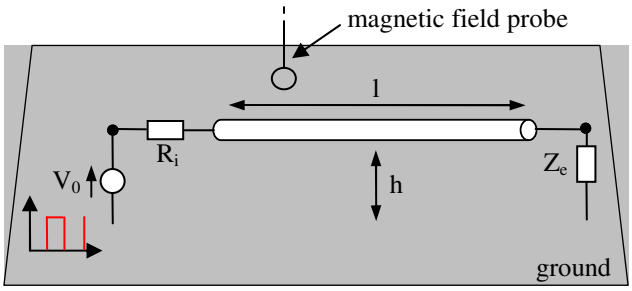

Figure 8. Single conductor under test

With the equivalent model radiations from the transmission line at any position and distance can be obtained. The electric far fields E_θ and E_φ are predicted and shown in Figure 9 and Figure 10, respectively. Exemplary the far fields of the 7th (f_1 = 60 MHz) and the 15th (f_2 = 124 MHz) harmonic of the pulsed input signal are presented. As a comparison a full field simulation of the cable under test given by a MoM solver [11] is shown. The two results agree in terms of pattern and amplitude with a maximum error of 2.5 dB at most angles.

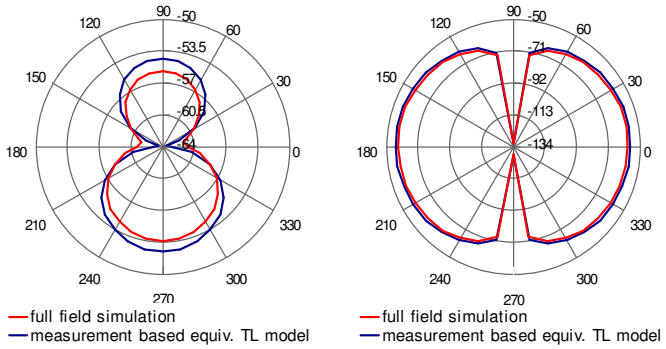

Figure 9. Electric far field (dBV/m) at distance r = 10 m (Left: E_θ, Right: E_φ), f_1 = 60 MHz

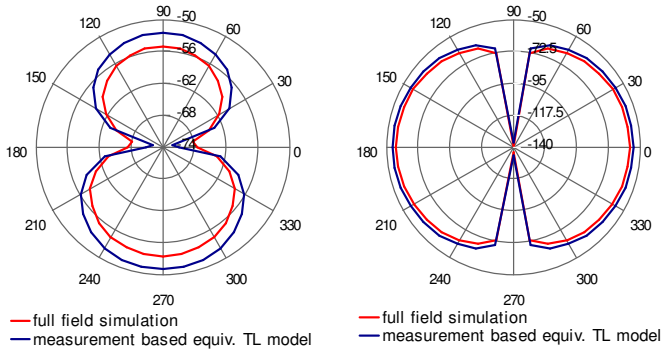

Figure 10. Electric far field (dBV/m) at distance r = 10 m (Left: E_θ, Right: E_φ), f_2 = 124 MHz

B. *Multiconductor –Equivalent Transmission Line Model*

The investigations for the multiconductor presently are done based on computer simulations.

The system (Figure 11) consists of a three single conductors with length l = 500 mm and thickness d = 1mm placed in the height h = 50 mm over a ground plane. The distance between the conductors is set to D = 10 mm. The transmission lines are terminated with Z_{e1} = 50 Ω, Z_{e2} = 150 Ω + s·1μH and Z_{e3} = 330 Ω. The excitation is impressed in the center line.

The predefined model parameters are adopted from the multiconductor. The internal resistance of the source is set to R_i = 50 Ω. The magnetic field is measured in two field points at a height h_S = 10 mm above the cable.

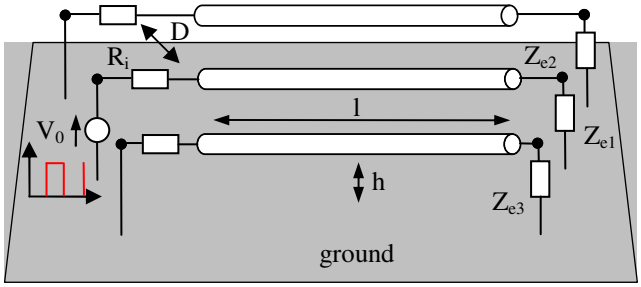

Figure 11. Multiconductor under test

In Figure 12 and Figure 13 electric far fields E_θ and E_φ are approximated with equivalent TL model and compared with a full field simulation. Here exemplary the far fields of the 5th (f_1 = 44 MHz) and the 7th (f_2 = 60 MHz) harmonic of the pulsed input signal are presented. The results agree in terms of pattern and amplitude with a maximum error of 3 dB at most angels.

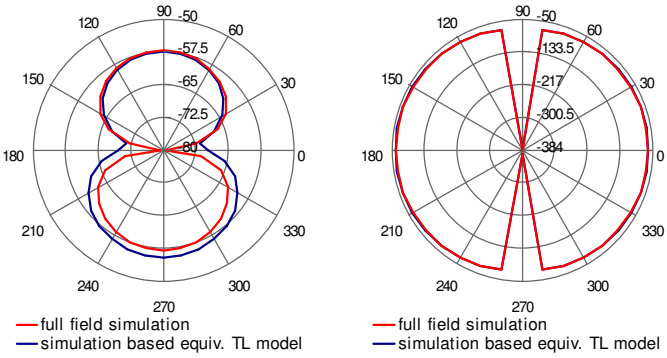

Figure 12. Electric far field (dBV/m) in distance r = 10 m (Left: E_θ, Right: E_φ), f_1 = 44 MHz

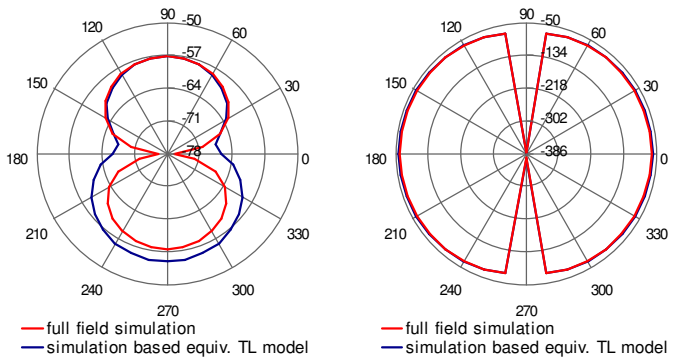

Figure 13. Electric far field (dBV/m) in distance r = 10 m (Left: E_θ, Right: E_φ), f_2 = 60 MHz

C. *Single Conductor – Equivalent Dipole Model*

The equivalent dipole investigations for the single conductor were done based on computer simulation.

The cable consists of a single conductor placed in the height $h = 5$ mm over a ground plane. It has a length of $l = 500$ mm and a thickness of $d = 1$ mm. It is terminated with a $Z_e = 50\ \Omega$ impedance. The predefined height of the dipole model is adopted from the cable. Figure 14 shows the magnetic field at a point 200 mm above the dipole arrangement in comparison with a full field simulation. The results agree with a maximum error of less 2 dB up to a frequency of 400 MHz.

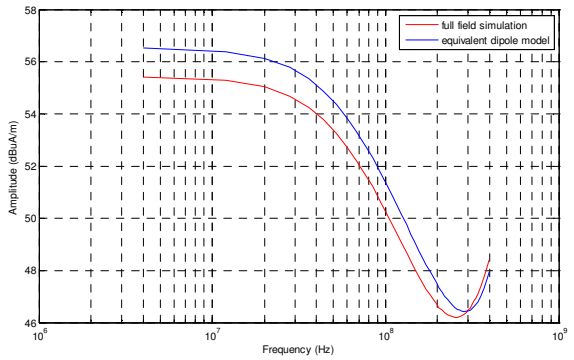

Figure 14. Magnetic field in height h = 200 mm above the cable

IV. CONCLUSION

In a frequency range up to 200 MHz radiation from cables is the dominant factor in automotive systems. Two methods to determine far-fields and simulation model of a radiating single cable or cable bundle were introduced in this paper. Methods are based on near field measurements of the magnetic field near the radiating cable. Measurements are done in Time Domain in order to get proper phase information and to decrease acquisition time. Applicability of Discrete Fourier Transformation (DFT) for post-processing is discussed and verified.

The approaches were tested by means of and in comparison to numerical full wave simulation data.

REFERENCES

[1] "CISPR 25 Ed.3: Vehicles, boats and internal combustion engines – Radio disturbance characteristics – Limits and methods of measurement for the protection of on-board receivers".

[2] Constantine A. Balanis, "Antenna Theory Analysis & Design", Wiley, 1996.

[3] Yolanda Vives Gilabert, "Modélisation des emissions rayonées de composants électroniques", Université de Rouen, 2007.

[4] D. Baudry, M. Kadi, Z. Riah, C. Arcambal, Y. Vives-Gilabert, A. Louis, B. Mazari, "Plane wave spectrum theory applied to near-field measurements for electromagnetic compatibility investigations", IET Science, Measurement and Technology, 15. June 2008.

[5] Tommaso Isernia, Giovanni Leone, Rocco Pierri, "Radiation Pattern Evaluation from Near-Field Intensities on Planes", IEEE Transaction on Antennas and Propagation, Vol. 44, No. 5, May 1996.

[6] Georg Monien, "Die Beeinflussung der Meßabweichung von Feldsonden und Stromzangen durch reale Umgebungsbedingungen", 2003.

[7] Edgar Voges, "Hochfrequenztechnik – Bauelemente, Schaltungen, Anwendungen", Hüthig Telekommunikation, 2004.

[8] G. Liu, D. J. Pommerenke, J. L. Drewniak, R. W. Kautz, C. Chen;, "Anticipating Vehicle-Level EMI Using A Multi-Step Approach", IEEE International EMC Symposium 2003

[9] S. Frei, T. Nägel, R. Jobava, "Bestimmung der Störaussendung im KFZ durch die getrennte Be-trachtung der elektrischen und magnetischen Verkopplungen", EMV Düsseldorf, 2004

[10] Spiegel, R., Booth, C., Bronaugh E., "A Radiation Measuring System with Potential Automotive Under-Hood Application", IEEE Transactions on Electromagnetic Compatibility, Vol. 25, No. 2, 1983, S. 61-69

[11] EMCoS Consulting and Software, "www.emcos.com"

[12] Xin Tong, D.W.P. Thomas, A. Nothofer, P. Sewell, C. Christopoulos, "A Genetic Algorithm Based Method for Modeling Equivalent Emission Sources of Printed Circuits from Near-Field Measurements", APEMC Beijing, 2010